MAGIICAT: The MgII Absorbing CGM of ~180 Galaxies

Nikole M. Nielsen[1], Christopher W. Churchill[1], Glenn G. Kacprzak[2], Sebastian Trujillo-Gomez[1], Michael T. Murphy[2]

[1]New Mexico State University, [2]Swinburne University of Technology

Nielsen et al. (arXiv:1211.1380, 1304.6716), Churchill et al. (2013) ApJ, 763, L42

astronomy.nmsu.edu/cwc/Group/magiicat

Introduction & Motivation

Inflowing and outflowing gas in galaxy halos is important in star formation and therefore galaxy evolution. Background quasar spectra provide sensitive absorption lines from these gaseous halos, known as the circumgalactic medium (CGM). The MgII λλ2796, 2803 doublet is ideal since it samples galaxies over the redshift range where the galaxies can be studied in detail. MgII is observed in outflowing winds (e.g., Weiner et al. 2009) and in infalling accretion (e.g., Rubin et al. 2012). Other studies have reported trends between MgII absorption and star formation rate, B-band luminosity, and/or stellar mass of the host galaxy (e.g., Chen et al. 2010; Ménard et al. 2011). Recent works indicate that the gas is preferentially located along the minor axis or the major axis of the host galaxy (e.g., Kacprzak et al. 2012), suggesting bipolar outflowing winds and coplanar accretion are the dominant structures traced by MgII absorption.

As such, increasing the sample size of known MgII absorbers and their host galaxies holds the promise of furthering our understanding of gas flows in galaxies. Many previous surveys have been published with samples no larger than ~80 galaxies. In many cases, magnitudes, colors, and quasar-galaxy projected separations are not directly comparable between samples due to differing cosmologies and magnitude systems. It is desirable to standardize previous surveys to form a large uniform sample of MgII absorption-selected galaxies.

MgII Absorber-Galaxy Catalog

We built a catalog of 182 isolated MgII absorption-selected galaxies (median z_{gal} = 0.36) taken from our work and a literature search. Figure 1 presents the quasar-galaxy offsets for most galaxies in MAGIICAT. We standardized all galaxy impact parameters and photometric properties to the current ΛCDM cosmology and placed all B- and K-band absolute magnitudes on the AB system using uniform K-corrections (see Kim et al. 1996) of the SEDs of Bolzonella et al. (2000). We also determined rest-frame B-K colors and B- and K-band luminosities. For details, see Nielsen et al. (2013).

Additionally, we applied halo abundance matching using the Bolshoi cosmological simulations (Trujillo-Gomez et al. 2011) to obtain halo masses, M_h, from absolute r-band magnitudes. We computed virial radii, R_{vir}, from the formalism of Bryan & Norman (1998). See Churchill et al. (2013) for details.

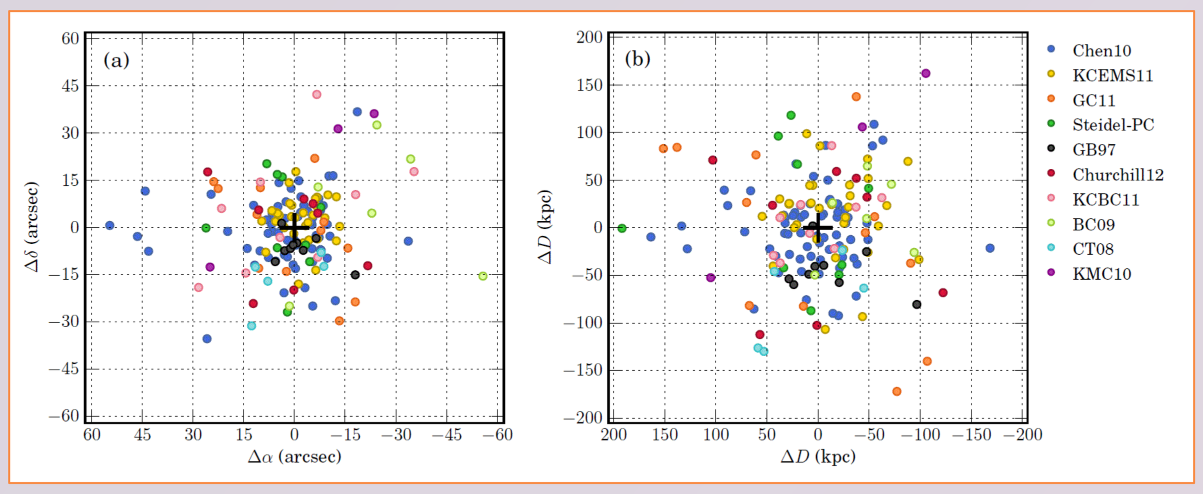

Figure 1 – Galaxy Offsets from the Background Quasars
Offsets in (a) angular, arcsec, and (b) physical, kpc, units of each galaxy for which we have measurements of Δα and Δδ from the associated background quasar (plus sign). Points are colored by the work from which the galaxy was obtained.

In Figure 2, we plot the MgII equivalent width, $W_r(2796)$, against D. $W_r(2796)$ is anti-correlated with D at the 7.9σ level (accounting for limits), indicating that the quantity of halo gas diminishes with projected distance. We find that the log-log fit from Chen et al. (2010) does not fit the overall trend of the data well due to the large number of galaxies with upper limits on absorption. A log-linear fit, $\log W_r(2796) = \alpha_1 D + \alpha_2$, is the best parameterization of the data, with $\alpha_1 = -0.015\pm0.002$ and $\alpha_2 = 0.27\pm0.11$. The considerable scatter about this relation suggests that $W_r(2796)$ is governed by physical processes related to the galaxy such as luminosity, star formation, or orientation. Churchill et al. (2013) find that the scatter has a strong dependence on the halo mass, M_h, and the scatter is greatly reduced when normalizing D by the virial radius.

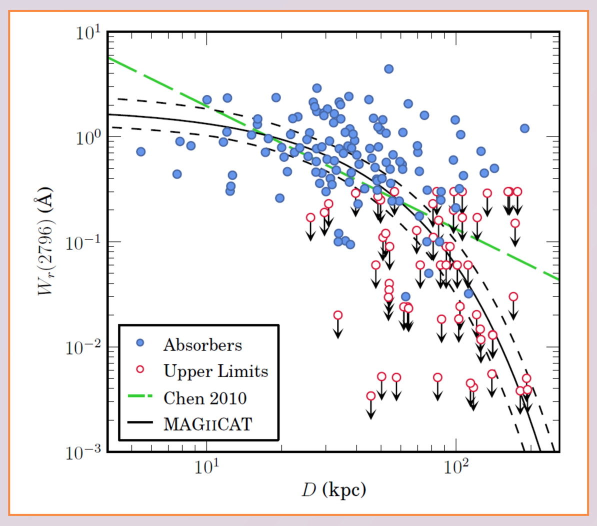

Figure 2 – $W_r(2796)$ vs D
The long dashed green line is the log-log fit to the data presented in Chen et al. (2010). The solid black line is a log-linear maximum likelihood fit to the data and the dashed curves provide 1σ uncertainties.

Absorption Gas Kinematics

Figure 3 presents the $W_r(2796)$ absorption profiles as a function of D for 50 galaxies in which $W_r(2796)$ was detected in HIRES/UVES spectra. The gas kinematics were modeled using Voigt profile fits (Evans 2011). The models are presented as red profiles. Galaxies with a limit in $W_r(2796)$ are not shown, but these additional ~30 galaxies provide further insights to the patchiness (covering fraction) of halos when included.

Luminosity Scaling

The outer boundary of absorbing gas is commonly assumed to follow a Holmberg-like relation, $R(L) = R_*(L/L^*)^\beta$. We examined whether the B- and K-band halo gas radius also depends on $W_r(2796)$. We apply four $W_r(2796)$ cuts and obtained R_* and β by maximizing the number of galaxies with $W_r(2796) \geq W_{cut}$ below the fitted line and maximizing the number of galaxies with $W_r(2796) < W_{cut}$ above the fitted line. In Figure 4, B-band results are presented. The scaling with L_B steepens from β ~ 0.3 to 0.4 at W_{cut} = 0.6 Å, where R_* ~ 90 kpc within uncertainties. The covering fraction decreases from $f_{R(L)}$ ~ 0.8 to 0.3 with increasing W_{cut}. For the K-band (not shown), β flattens slightly from 0.2 to 0.15 and R_* decreases from 75 kpc to 60 kpc. The covering fraction behaves similarly to the B-band.

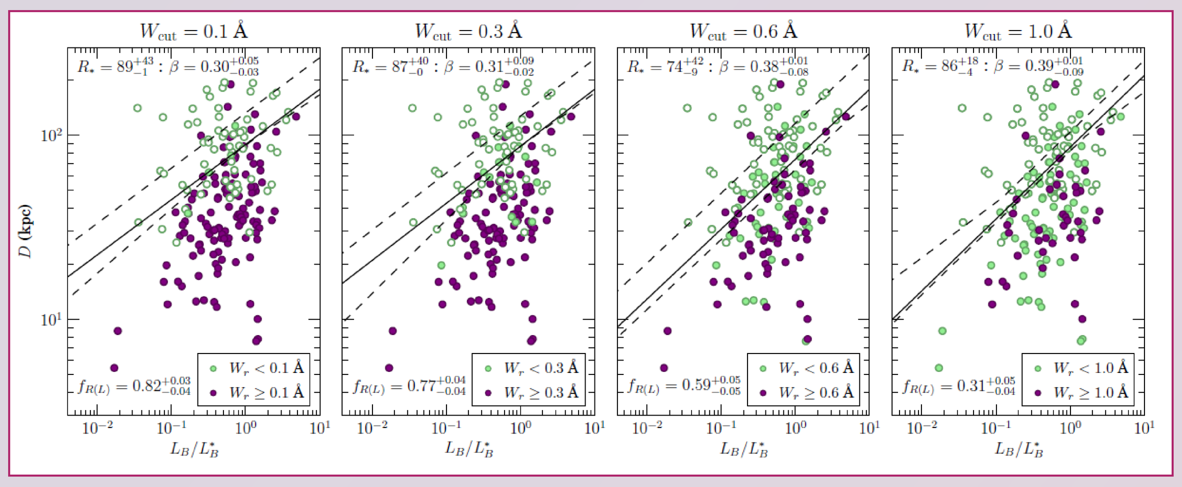

Figure 4 – D vs L_B for Different $W_r(2796)$ Bifurcations
In each panel, purple points are galaxies that have a measured $W_r(2796) \geq W_{cut}$ and green points are galaxies with $W_r(2796) < W_{cut}$. Open points represent galaxies which have limits on $W_r(2796)$. Dashed lines provide the 1σ uncertainties in the fit.

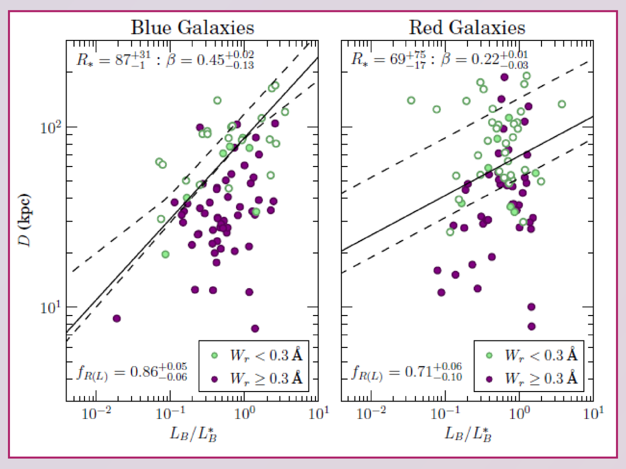

For the B-band, we compare R_*, β, and $f_{R(L)}$ between red and blue galaxies for W_{cut} = 0.3 Å, which we illustrate in Figure 5. Blue galaxies have a larger halo absorption radius, steeper luminosity scaling, and larger covering fraction than red galaxies.

Figure 5 – D vs L_B for Red and Blue Galaxies
Galaxies were sliced by blue (B-K < 1.49) and red (B-K ≥ 1.49) colors for W_{cut} = 0.3 Å. The point and line types in Figure 4 apply here.

Covering Fraction

We calculated the covering fraction profile of the MgII CGM with projected distance from the galaxy by determining the fraction of absorbers with $W_r(2796) \geq W_{cut}$ in fixed impact parameter bins. The covering fraction profiles for the full sample and for high and low luminosity subsamples cut by L_B/L_B^* = 0.549 are shown in Figure 6. The covering fraction decreases with increasing D and with increasing W_{cut}. High luminosity galaxies have larger covering fractions at all impact parameters, and low luminosity galaxies have no absorption outside D = 200 kpc.

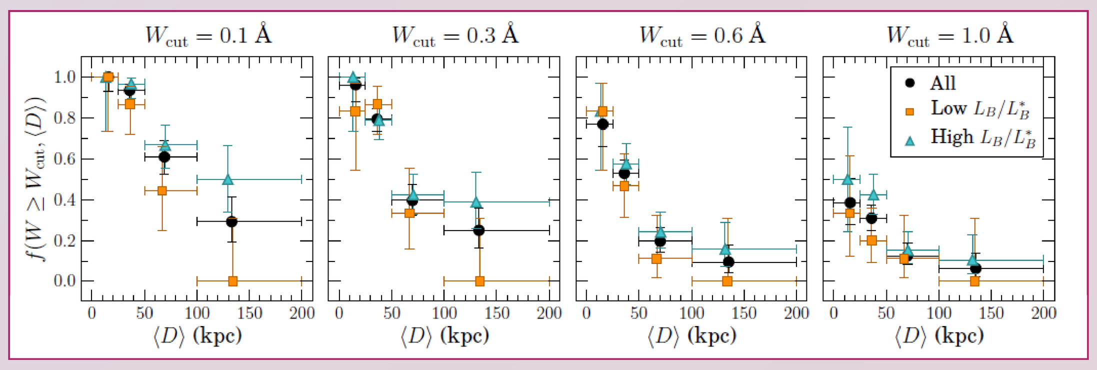

Figure 6 – Covering Fraction Profiles The covering fraction profile for different D bins and $W_r(2796)$ thresholds. Horizontal bars indicate the D bin width and vertical bars are 1σ binomial uncertainties. Points are plotted at the mean D for each bin for the full sample of MAGIICAT galaxies and high and low B-band luminosity galaxies.

Splitting the sample by galaxy color (B-K = 1.49) and redshift (z_{gal} = 0.359) in Figure 7, we find that there is no difference in $f_{\langle D \rangle}$ between red and blue galaxies, but higher redshift galaxies have larger covering fractions at all D.

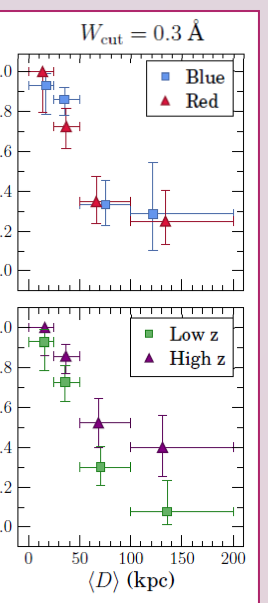

Figure 7 – Covering Fraction Profiles
The covering fraction profile for B-K and z_{gal} subsamples. Horizontal and vertical bars are the same as those in Figure 6.

We also calculated the covering fraction within a fixed D for different halo mass bins as shown in Figure 8. We find the covering fraction does not vanish for $\log (M_h/M_\odot) \gtrsim 12$, contrary to theoretical predictions for cold-mode accretion (e.g., Stewart et al. 2011, van de Voort et al. 2011).

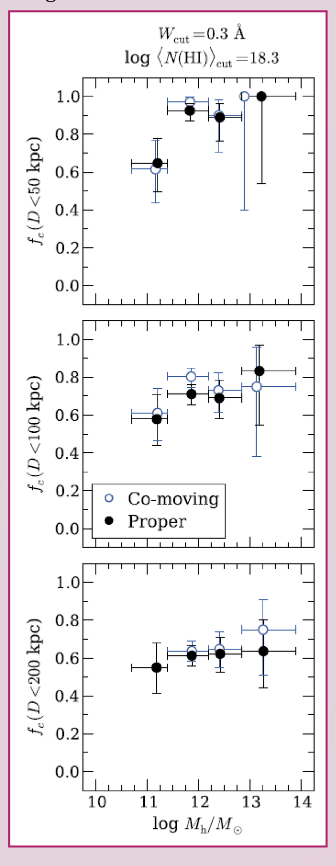

Figure 8 – Covering Fraction vs Mass
The covering fraction within a maximum D for different halo mass bins. Horizontal and vertical bars are the same as those in Figure 6.

Cloud-Cloud Velocity Clustering

Using the sample of 42 MgII absorption profiles in HIRES/UVES spectra associated with MAGIICAT galaxies presented in Figure 3, we determine the two-point velocity correlation function (TPCF), which is the probability of finding any two clouds separated by a particular velocity difference Δv. We calculated the TPCF for various subsamples sliced by galaxy rest-frame color, redshift, halo mass, impact parameter, and virial radius-scaled impact parameter as shown in Figure 9. In every case, statistical tests (Chi-square test on binned data, and the f-test and Kolmogorov-Smirnov test on unbinned data) between the two subsamples show that the TPCFs of the two subsamples are not drawn from the same population to greater than the 10σ level.

Figure 9a presents the TPCF for red and blue galaxies. Blue galaxies have a more extended high velocity separation tail while red galaxies are peaked at low velocity separations and this difference is accentuated when velocities are normalized by V_{circ}. In Figure 9b, higher redshift galaxies have more extended tails than low redshift galaxies, which are dominated by low velocity separations.

Figure 9 – TPCFs for Various Subsamples Split by Galaxy Properties
Solid lines are the TPCF while the shading around the solid line represents the 1σ Poisson uncertainties. Left panels present the TPCF for Δv separations while right panels present the TPCF for velocity separations where v is normalized by V_{circ} to account for the galaxy halo mass.

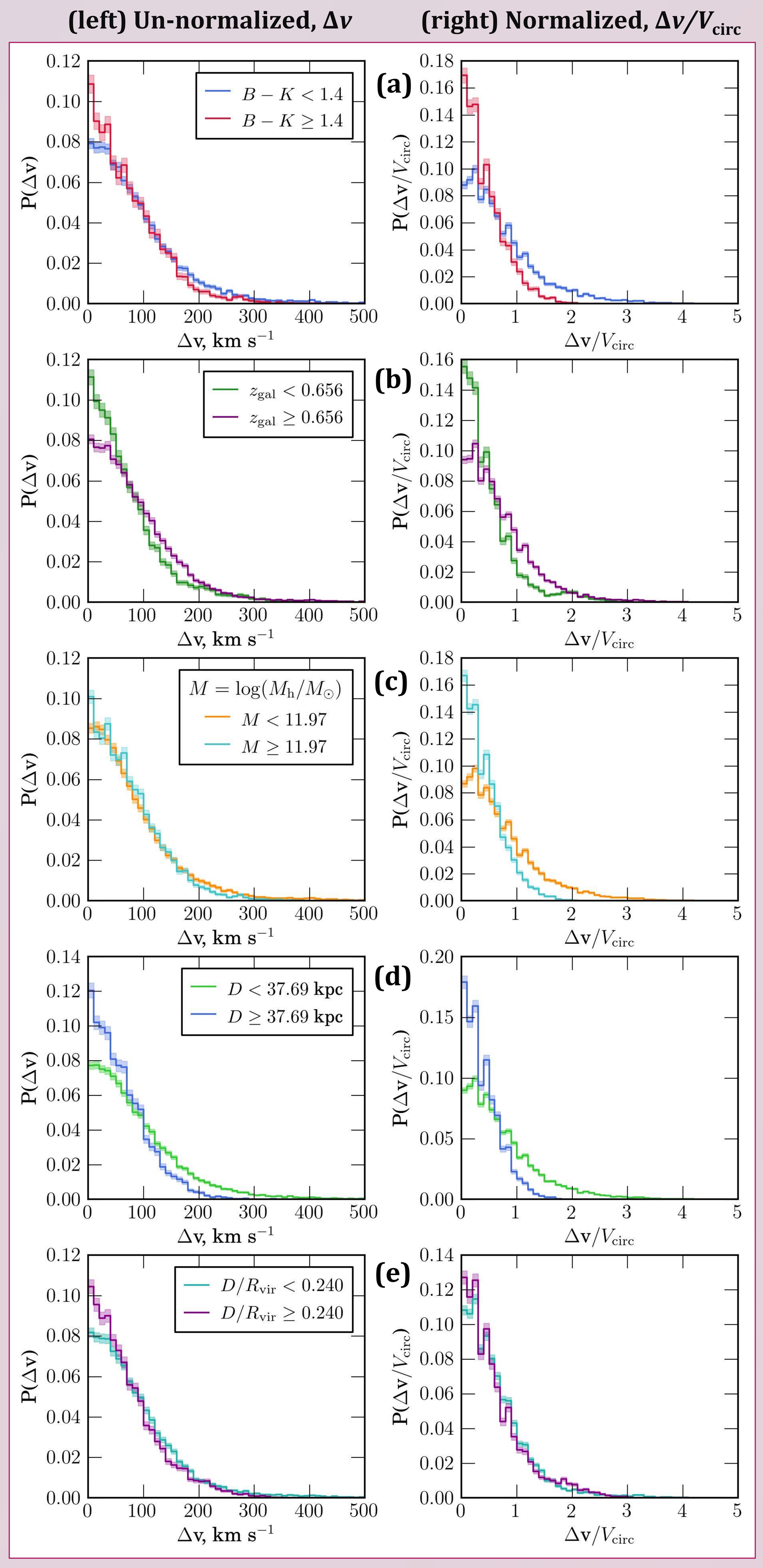

Panel (a): Galaxy rest-frame B-K color

Panel (b): Galaxy redshift, z_{gal}

Panel (c): Halo mass, M_h

Panel (d): Impact parameter, D

Panel (e): Impact parameter normalized by the galaxy virial radius, D/R_{vir}

In Figure 9c, high and low mass galaxies appear to show no differences in their TPCFs for Δv, but for $\Delta v/V_{circ}$, the TPCF is more extended for low mass galaxies than the more centrally peaked high mass galaxies. Galaxies whose CGM is probed at low impact parameters have large cloud-cloud velocity separations as indicated in Figure 9d, while large impact parameter galaxies are dominated by small velocity separations. Finally, there appears to be no differences in the TPCFs for galaxies probed at large and small D/R_{vir} as indicated in Figure 9e.

References

Bolzonella, M., Miralles, J.-M., & Pelló, R. 2000, A&A, 363, 476
Bryan, G. L., & Norman, M. L. 1998, ApJ, 495, 80
Churchill, C. W., Nielsen, N. M., Kacprzak, G. G., Trujillo-Gomez, S. 2013, ApJ, 763, L42
Evans, J. L. 2011 Ph.D. Thesis, New Mexico State University
Kacprzak, G. G., Churchill, C. W., & Nielsen, N. M. 2012, ApJ, 760, L7
Kim, S., Goobar, A., & Perlmutter, S. 1996, PASP, 108, 190
Ménard, B., et al. 2011, MNRAS, 417, 801M
Nielsen, N. M., Churchill, C. W., & Kacprzak, G. G. 2012, arXiv:1211.1380 (Paper II)
Nielsen, N. M., Churchill, C. W., Kacprzak, G. G., & Murphy, M. T. 2013, arXiv:1304.6716 (Paper I)
Rubin, K. H. R., Prochaska, J. X., Koo, D. C., & Phillips, A. C. 2012, ApJ, 747L, 26R
Stewart, K. R., Kaufmann, T., Bullock, J. S., et al. 2011, ApJL, 735, 1
Trujillo-Gomez, S., Klypin, A., Primack, J., & Romanowsky, A. J. 2011, ApJ, 742, 16
van de Voort, F., Schaye, J., Booth, C. M., Haas, M. R., & Dalla Vecchia, C. 2011, MNRAS, 414, 2458
Weiner, B. J., et al. 2009, ApJ, 692, 187W

The following papers were included in our literature search:
Chen, H.-W., Helsby, J. E., Gauthier, J.-R., Shectman, S. A., Thompson, I. B., & Tinker, J. L. 2010a, ApJ, 714, 1521 (Chen10)
Chen, H.-W., & Tinker, J. L. 2008, ApJ, 687, 745 (CT08)
Churchill, C. W., Kacprzak, G. G., Nielsen, N. M., Steidel, C. C., & Murphy, M. T. 2013, ApJ, submitted (Churchill13)
Gauthier, J.-R., & Chen, H.-W. 2011, MNRAS, 418, 2730 (GC11)
Guillemin, P., & Bergeron, J. 1997, A&A, 328, 499 (GB97)
Kacprzak, G. G., Churchill, C. W., Barton, E. J., & Cooke, J. 2011, ApJ, 733, 105 (KCBC11)
Kacprzak, G. G., Churchill, C. W., Evans, J. L., Murphy, M. T., & Steidel, C. C. 2011, MNRAS, 416, 3118 (KCEMS11)
Kacprzak, G. G., Murphy, M. T., Churchill, C. W. 2010, MNRAS, 406, 445 (KMC10)
Steidel, C. C., Dickinson, M., Meyer, D. M., Adelberger, K. L., & Sembach, K. R. 1997, ApJ, 480, 568 (Steidel97)
Steidel, C. C., Dickinson, M., & Persson, S. E. 1994, ApJ, 437, L75 (SDP94)

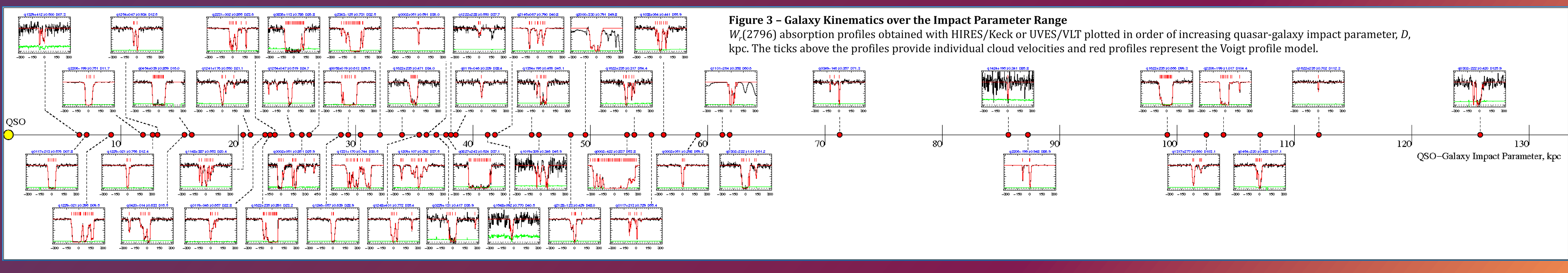

Figure 3 – Galaxy Kinematics over the Impact Parameter Range
$W_r(2796)$ absorption profiles obtained with HIRES/Keck or UVES/VLT plotted in order of increasing quasar-galaxy impact parameter, D, kpc. The ticks above the profiles provide individual cloud velocities and red profiles represent the Voigt profile model.